ISSN: 1394-7990
Malaysian Journal of Soil Science Vol. 24: 65-81 (2020) Malaysian Society of Soil Science

Accelerated Weathering of Secondary Minerals on Ratu Crater Toposequences of Tangkuban Parahu Volcano, West Java

Hakim, D.L.[1,*], McDaniel, P.[2] and Kamarudin, K.R.[3]

[1]Faculty of Agriculture, Universitas Galuh, District of Ciamis, West Java 46215, Indonesia
[2]College of Agricultural and Life Sciences, University of Idaho, Moscow, ID 83844, USA
[3]Faculty of Applied Sciences and Technology, UTHM, 84600 Muar, Johor, Malaysia

ABSTRACT

The crater environment of Ratu Crater, Tangkuban Parahu Volcano was largely shaped by chemical processes that occurred in the geothermal centre in the form of fumarole and solfatar. A range of five representative profiles were identified in the toposequences of the crater i.e. A (toeslope), B, D (backslope), G and J (summit). Soil samples were physically, chemically, and mineralogically analysed. Mineralogical analysis showed that the sand fraction of heavy minerals (specific gravity> 2.87) were opaque, augite, and hipersten, while light minerals (specific gravity< 2.87) were volcanic glass, zeolite, andesin, labradorite, bitownite and rock fragments. Extraction with oxalate and pyrophosphate showed Profile D (backslope) to contain the highest mineral content of allophane (1.414 %), imogolite (0.391 %), and ferrihydrite (2,091 %). The lowest content was found in Profile A (toeslope), which had a smaller content than Profile J (summit). XRD analysis results (no treatment) showed that all profiles of A, B, D, G, J had almost the same reflection pattern consisting of calcite (3.03 Å), cristobalite (4.04 Å), feldspar (3.1-3.25 Å, gibbsite (4.85 Å), kaolinite (7.1 Å) and quartz (3.34, 4.27 Å). XRD analysis (Mg+glycol) of the profiles showed each profile to be mostly dominated by non-crystalline minerals (amorphous); however Profile J (Summit) and Profile A (toeslope) were dominated by crystalline minerals that had been developed from amorphous minerals, i.e. mineral 2:1 (smectite and chlorite) and mineral 1:1 (halloysite and kaolinite).

Key words: Crater, secondary minerals, geothermal, toposequences, volcanic ash.

INTRODUCTION

Tangkuban Perahu volcano, located in West Java, is one of the active volcanoes in Indonesia. Tangkuban Perahu is a post-caldera volcano situated in the eastern rim of the Sunda caldera. A number of research studies have been conducted on Tangkuban Perahu volcano. However, they only observed the geologic condition

*Corresponding author : E-mail: *danijudge@yahoo.com*

of the volcano and the soil genesis developed in the external system. A crater is a volcanic depression formed as a result of explosion and is integral to the volcano's internal system. The mineral development inside the crater remains unclear to date.

The clay mineralogy of the soils formed in volcanic materials varies widely depending on factors such as the composition of the parent material, stage of soil formation, pH, soil moisture regime, and the accumulation of organic matter (Shoji 1985). Poorly ordered materials such as allophane, imogolite, ferryhydrite, and Al- and Fe-humus complexes often dominate the clay size fraction of volcanic soils.

Generally, climatic conditions and their effects on degree of leaching and soil solution chemistry also play an important role in volcanic material weathering pathways and secondary mineral neogenesis. Volcanic materials may weather directly to short range order (SRO) materials or kaolin, depending on the amount of rainfall and silica solution activity (Parfitt *et al*. 1983). Kaolin minerals can show a wide range of structural disorder (Churchman 1990; Soma *et al.* 1992) due primarily to Al-vacancy displacements in the octahedral sheet (Soma *et al.* 1992). These vacancies may originate from non-stoichiometric substitution of Fe^{3+} for Al^{3+} in the octahedral sheet (Soma *et al.* 1992). Indeed, some studies have shown that crystalline clays, such as halloysite, form initially without a SRO precursor in weathering systems that exhibit high solution silica activity (McIntosh 1979; Singleton *et al*. 1989). Variable effects of hydration might also add to the degree of disorder in halloysite. Low rainfall or leaching promote a high solution of silica activities and facilitate halloysite formation, whereas high precipitation or leaching promote low silica activities, favoring SRO minerals (Parfitt *et al*. 1983). Likewise precipitation and temperature also play a role in the formation of SRO or crystalline minerals, which promotes crystallisation as the soil climate gets warmer and drier (Talibudeen and Goulding 1983; Schwertmann 1985). SRO minerals are more persistent under low soil temperatures as crystallisation is hindered by a low input of thermal energy. Therefore, we hypothesised that thermal energy radiated by sulphide existing in the crater affected the transformation of the minerals surrounding the crater, and the translocation process. This study was done to investigate the formation of secondary minerals across Ratu Crater toposequences of Tangkuban Parahu volcano, West Java.

MATERIALS AND METHODS

Environmental Setting

A series of volcanic ash material were examined on the topographic gradient of Ratu Crater (toposequences). The transect spun a broad environmental gradient with variations in slope level.

Field Methods

In this study, five representative sample profiles (A, B, D, G, J) were taken along the path of the Ratu Crater topographic gradient (toposequences) of Tangkuban Parahu volcano (Figure 1) with a steep to very steep slope grade (Van Zuidam 1986). The observation and discussion focus only on the data taken from five profiles i.e. Profile A-toeslope, Profile B , Profile D-backslope, Profile G and Profile J-summit (Figure 2). Samples from each profile were analysed for physical, chemical, and mineralogical properties. All samples were dominated by volcanic ash parent material, released by Tangkuban Parahu volcano eruption.

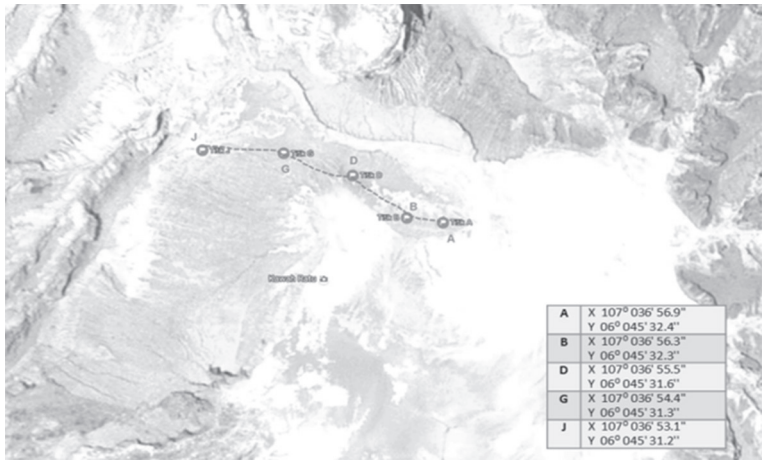

Figure 1. 3D illustration of sample profile distribution on Ratu Crater toposequences. The image was taken from the eastern top of Ratu Crater: Profile A (toeslope), Profile D (backslope), and Profile J (summit)

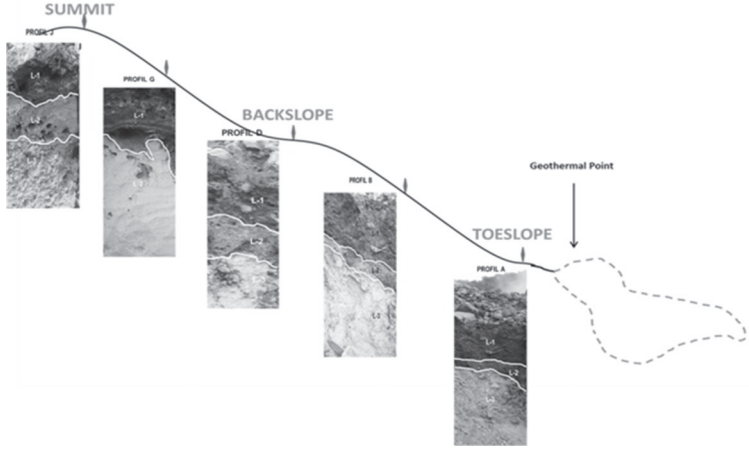

Figure 2. Cross-section illustration of sample profile distribution on Ratu Crater toposequences: Profile A (toeslope), Profile D (backslope), and Profile J (summit)

Laboratory Methods

Physical Analysis

Samples were air-dried and crushed to pass a 2-mm sieve. Coarse (2.0–0.2 mm), fine-sand (0.20–0.02 mm), silt (0.020–0.002 mm), and clay (0.002 mm) fractions were separated by pipette and sieving following pretreatment with H_2O_2 to oxidise organic matter and dispersion aided by sodium hexa-metaphosphate. Water content at 1.5 MPa was determined on air-dried and field-moist 2-mm soil (Soil Survey Staff 2014).

Chemical Analysis

Soil pH was measured by potentiometry in soil/solution suspensions of 1:2.5 H_2O and 1:2.5 1−MKCl. Organic C (OC) was estimated by wet digestion with a modified Walkley-Black procedure (Tan, 2010).

Mineralogical Analysis

X-ray diffraction (XRD) was performed on the clay (<2 μm), silt (2–53 μm), and very fine sand (53–100 μm) fractions for each horizon of the some pedon in the observation line. Clays and silts were collected by repeated mixing and centrifugation with dilute Na_2CO_3. X-ray analyses were done with a Diano XRD 8000 diffractometer (Diano, Woburn, MA).

Clays and silts were oriented on glass slides with the following standard treatments: Mg saturation, Mg saturation and glycerol solvation (Whittig and Allardice 2018). Halloysite was distinguished from kaolinite by the presence of a peak near 1.0 nm after intercalation with formamide (Churchman 1990). Very fine sands were analysed using random powder mounts.

Selective dissolution was performed on the fine-earth fraction by non-sequential extractions using sodium pyrophosphate, acid ammonium oxalate, and citrate–dithionite (Soil Survey Staff 2014). Samples were shaken for 15 h with 0.1−M sodium pyrophosphate at pH 10 and a soil/liquid ratio of 1:100 to extract Al (Al_p) bound in organo-metal complexes. Samples were shaken for 4 h in the dark with a soil/oxalate ratio of 1:100 with 0.2-Mammonium oxalate adjusted to pH 3.0 with oxalic acid to extract Al, Fe, and Si (Al_o, Fe_o, and Si_o) from organic complexes and SRO Fe oxyhydroxides (e.g. ferrihydrite) and aluminosilicates (e.g. allophane and imogolite).

Citrate-dithionite extraction consisted of shaking 4g of soil for 15 h with 2g of sodium dithionite and 100 mL of 0.3-M sodium citrate to extract Fe and Al (Fe_d and Al_d) from organic complexes, some SRO aluminosilicates, and secondary forms of Fe oxyhydroxides (Parfitt and Childs 1988; Dahlgren 1994). Aluminum and Fe concentrations were determined by atomic absorption spectrophotometry, and Si was determined by colorimetry (Weaver *et al.* 1968).

All laboratory analyses were carried out at Pedology Laboratory, University of Idaho (Moscow, USA); Soil Research Institute, Bogor; Geology Laboratories, Bandung; and Laboratory of Soil Chemistry and Plant Nutrition, Padjadjaran University.

RESULTS AND DISCUSSION

Soil Physical Properties

Texture

The texture analysis showed that the sand and silt fractions dominated almost all sample profiles (Table 1). A small amount of clay fraction was found. Some profiles had clay content of below 5%. Interestingly, allophane in the clay fraction was the main mineral of the soil even though the clay fraction was only below 5%.

Though the results of the texture analysis may not reflect the actual conditions, the texture at the location was dominated by sand and silt fractions, thus the class textures were from loam to sandy loam. The composition order of soil fractions in each profile was sand>silt> clay, while the clay composition in each profile was J> D> A> B> G.

TABLE 1
Soil texture analysis on each sample profile

Profile	Sand	Silt	Clay	Total fraction
		(%)		
A	61.62	32,.01	6.37	Sandy loam
B	60.44	35.80	3.76	Sandy loam
D	73.49	20.09	6.42	Loamy sand
G	81.54	15.09	3.37	Loamy sand
J	42.96	45.10	11.94	Loam

Soil Chemical Properties

pH Value

The pH values of soil in H_2O ranged between 2.71 and 5.51 and showed a distinct trend with increasing elevation (Table 2). This was in contrast to similar elevation gradients on granite and basalt parent materials ranges, where pH steadily declined with increasing elevation (Dahlgren *et al.* 1997). Besides, the pH values in KCl ranged between 2.33 and 4.16 showing a similar trend with the pH values in H_2O.

TABLE 2
pH values of soil (in H_2O and KCl) in sample profiles along the Ratu Crater toposequences

Profile	H_2O	KCl	Δ pH
A	2.71	2.33	-0.38
B	3.65	3.05	-0.60
D	3.68	3.05	-0.63
G	4.80	4.16	-0.64
J	5.51	4.16	-1.35

The geothermal system must have played an important role in the trend due to the presence of rich sulfuric acid, indicating major amounts of exchangeable H^+ (Tan 2010). Delta pH values [$\Delta pH = pH(KCl) - pH(H_2O)$] ranged between -0.38 and -1.35, indicating that all sites were dominated by a net negative surface charge (Soil Survey Staff 2014). The unexpectedly high pH in the upper elevation sites may be a result of decreased leaching, probably because the leaching process by precipitation may not have infiltrated the soil profile.

Organic Carbon

Soil organic C content (on a mass percentage basis) on the upper horizon showed no clear pattern (Table 3). Soil C content variation across the gradient was probably due to the presence of SRO materials that provided numerous adsorption sites for C coupled with the Al-humus complex that inhibits biodegradation of organic C (Parfitt and Kimble 1989; Rasmussen *et al.* 2007).

TABLE 3
The chemical composition of soils along the Ratu Crater toposequence

Profile	S	Fe	Pyrite (FeS_2)	C Org
			(%)	
A	0.10	0.02	0.04	0.73
B	0.09	3.04	0.17	0.63
D	0.14	2.13	0.26	0.40
G	0.22	0.07	0.14	0.43
J	0.16	2.18	0.30	2.65

Soil Mineralogical Properties

Quantitative Analysis of Sand Fraction Minerals

Mineralogical analysis of the sand fraction showed that the heavy minerals (specific gravity > 2.87) were opaque, augite, and hyperstein at various percentages (Table 4). Light minerals (specific gravity < 2.87) found were volcanic glass, zeolite, andesine, labradorite, bitownite and rock fragments.

Volcanic Glass

Volcanic glass content varied substantially across the gradient (Figure 3) and the pattern may be due to a function of differential weathering environments or parent material variation, or both. This variation in glass content suggests that glass was accumulated by the leaching process from the top to bottom gradient, due either to precipitation or gravitational energy. Glass content increased significantly in Profile A, suggesting a possible accumulation threshold related to the form of slope gradient.

TABLE 4
The mineral composition of soils along the Ratu Crater toposequence

Profile	Heavy mineral (%)			Light mineral (%)				LM
	Op	Aug	Hip	GV	Lab	Bit	FB	
A	0	0	0	96	0	0	3	1
B	3	6	2	63	16	2	4	4
D	2	6	1	61	22	1	5	2
G	0	0	0	98	0	0	0	2
J	3	7	0	64	20	0	2	4

Op= opaque
Aug= augite
Hip = hypersteine
GV = volcanic glass
Lab = labradorite
Bit= bitownite
FB = rock fragment
LM = altered mineral

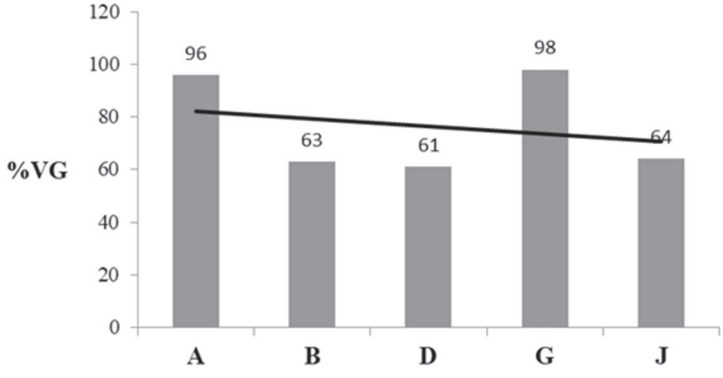

Figure 3. Volcanic glass content in the very fine sand (VFS) fraction of surface horizon on gradient from toeslope (Profile A) to summit (Profile J)

Profiles B, D, and J showed less glass content compared to Profiles A and B, probably a result of enhanced leaching due to the degree of the gradient slope. It is also possible that some volcanic glasses in the lower slope originated from the latest volcanic eruptions as the glass also showed resistance to chemical weathering (Shoji 1985). The linear line in Figure 3 suggests that the content of volcanic glasses decreased from lower to higher gradient slope.

XRD on Silt and Very Fine Sand Fraction

Samples were selected from three profiles representing extreme different gradients i.e. Profile A as toeslope, Profile D as backslope, and Profile J as summit. XRD analysis (without treatment) on silt and very fine sand fraction (Figure 4) showed that all profiles contained almost similar reflection patterns showing the presence of calcite (3.03 Å), cristobalite (4.04 Å), feldspar (3.1-3.25 Å, gibbsite (4.85 Å), kaolinite (7.1 Å) and quartz (3.34, 4.27 Å) (Table 5).

TABLE 5
Mineral composition of each profile based on the results of XRD analysis on silt and very fine sand fraction

Profile	Mineral
A	Feldspar ($KAlSi_3O_8$ – $NaAlSi_3O_8$ – $CaAl_2Si_2O_8$) Cristobalite (SiO_2) Quartz (SiO_2)
B	Feldspar ($KAlSi_3O_8$ – $NaAlSi_3O_8$ – $CaAl_2Si_2O_8$) Cristobalite (SiO_2) Quartz (SiO_2)
D	Feldspar ($KAlSi_3O_8$ – $NaAlSi_3O_8$ – $CaAl_2Si_2O_8$) Quartz (SiO_2)
G	Feldspar ($KAlSi_3O_8$ – $NaAlSi_3O_8$ – $CaAl_2Si_2O_8$) Gibbsite ($Al(OH)_3$) Quartz (SiO_2)
J	Feldspar ($KAlSi_3O_8$ – $NaAlSi_3O_8$ – $CaAl_2Si_2O_8$) Calcite ($CaCO_3$) Gibbsite (Al (OH)3) Kaolinite (Al_2O_3 $2SiO_4.2H_2O$) Cristobalite (SiO_2) Quartz (SiO_2)

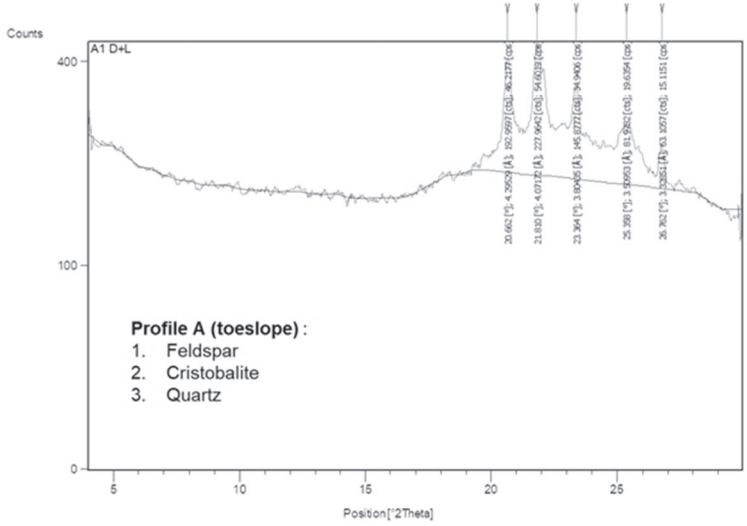

(a)

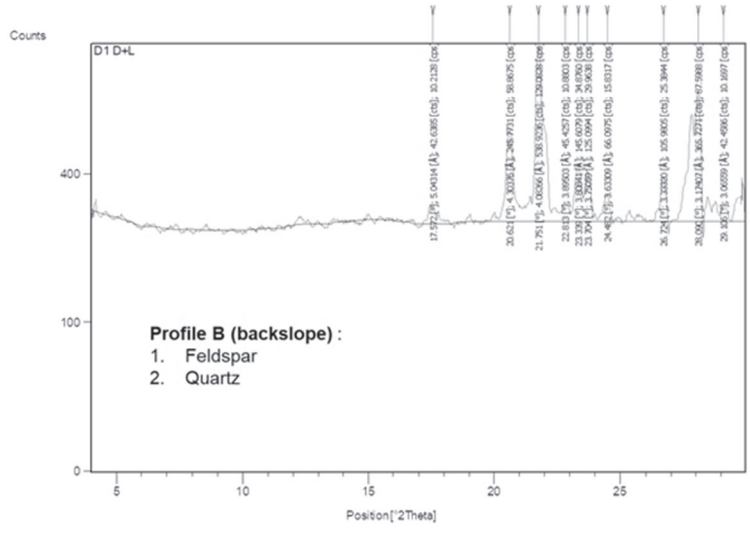

(b)

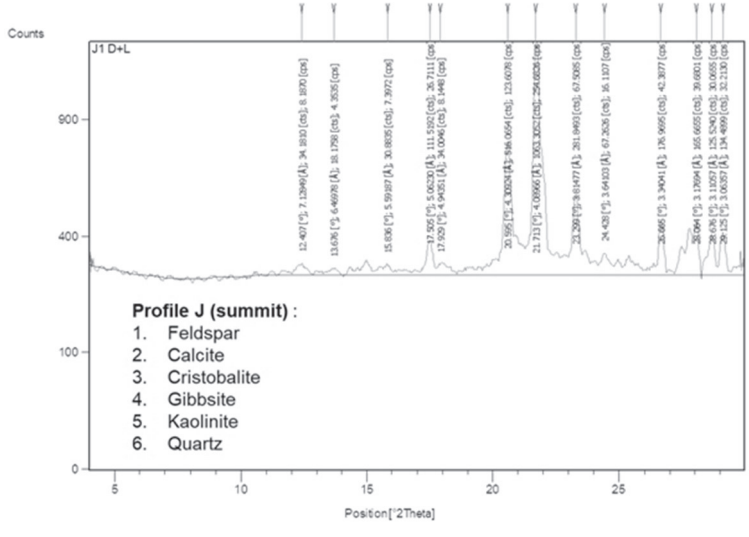

(c)

Figure 4. Images from XRD analysis (no treatment) on silt and very fine sand fractions from surface horizons of each profile; (a) Profile A (toeslope), (b) Profile D (backslope), and (c) Profile J (summit)

Microscopic Analysis

Polarisation Microscope

Polarisation microscopic observations on very fine sand fractions showed that all sample profiles had fresh volcanic glass indicated by bright colours, while other parts had weathered indicated by dark colours (Figure 5). However, most weathered minerals were found at A (toeslope) point, and D (backslope) point, and least amounts at J point (summit).

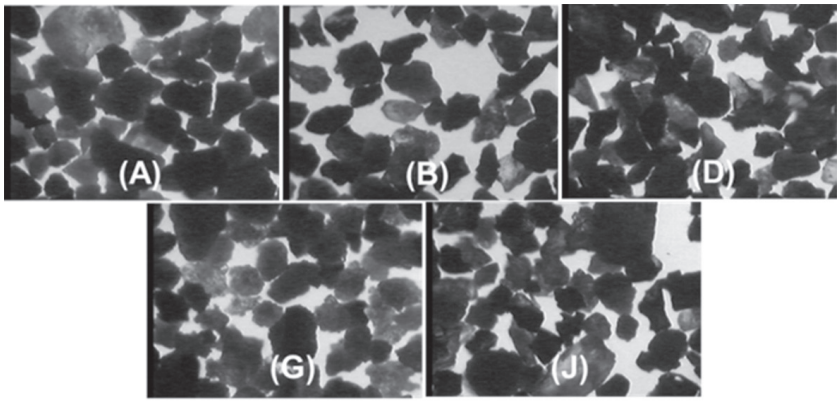

Figure 5. Images from polarisation microscopic observations on very fine sand with 40x magnification; (A), (B), (D), (G), and (J) indicate respective profiles

In fact, A point was a place of accumulated materials. Furthermore, A point had specific environmental characteristics in terms of temperature and pH due to geothermal activities of the crater. The volcanic glass content of the soil was very dependent on the content of the initial volcanic glass and the level of weathering. The higher level of weathering in soil had resulted in less volcanic glass content due to its transformation into both crystalline minerals and secondary minerals (Van Ranst *et al.* 2016).

Quantitative Analysis with Oxalate and Pyrophosphate Selective Solutions

The results of the analyses with oxalate and pyrophosphate acid are shown in Table 6. Silica, aluminum and iron extracted with oxalate and pyrophosphate acid were symbolised as Si_o, Al_o, Fe_o, Si_p, Al_p, and Fe_p. The percentages of allophane, imogolite and ferihydrite were calculated based on the amounts of Si, Al, and Fe extracted with oxalate and pyrophosphate acid with the equation proposed by Shoji (1985) as follows: (1) % allophane = % Si_o x 7.14; (2) % imogolite = % (Al_o – Al_p) x 1.7; (3) % ferihydrite = % Fe_o x 1.7. The Al_o value was higher than that of Al_p because oxalic acid extracted Al derived from allophane, imogolite and Al-humus complex while pyrophosphate only extracted Al from the Al-humus complex. The presence of non-inorganic crystalline Al was estimated from the difference in Alo-Alp. Table 6 shows that Al_o-Al_p values ranged from

0.10-0.23%, suggesting the tendency of the profile on the upper slope to have a higher value than the profile on the lower slope in the internal environment of the crater. This result indicates that the proportion of Al-humus complexes decreases and the Al-inorganic form increases, corresponding to the depth of the crater. An opposite relationship was observed in the case of the formation of Al-humus with Al-inorganic (allophane, imogolite, ferihydrite). The presence of humus inhibited allophane formation (non allophanic reaction) if the content of organic matter was high.

TABLE 6
Extraction results with oxalate and pyrophosphate acid and percentage estimation of allophane, imogolite, and ferihydrite (%)

Profil	Si_o	Al_o	Fe_o	Al_p	Fe_p (%)	$Al_o + ½ Fe_o$	Al_o-Al_p	al	im	fer
A	0,003	0,02	0,02	0,01	0,02	0,030	0,01	0,021	0,017	0,034
B	0,074	0,15	0,03	0,05	0,12	0,165	0,10	0,528	0,170	0,051
D	0,198	0,34	1,23	0,11	0,04	0,955	0,23	1,414	0,391	2,091
G	0,001	0,03	0,04	0,01	0,02	0,050	0,02	0,007	0,034	0,068
J	0,070	0,20	1,55	0,08	0,06	0,975	0,12	0,500	0,204	2,635

al = allophone; im = imogolite; fer = ferihydrite

XRD on Clay Fraction

The XRD analysis (Mg+glycol) on clay fraction showed that each profile was dominated by amorphous materials. Profile J (Summit) and Profile A (toeslope) were dominated by crystalline minerals that could have been developed from the amorphous materials i.e. mineral 2: 1 (smectite and chlorite) and mineral 1:1 (halloysite and kaolinite).

Based on the analysis results, this study showed that crystalline clays such as halloysite were formed initially without a SRO precursor in weathering systems that exhibited high solution silica activity (McIntosh 1979; Singleton *et al.* 1989). Variable effects of hydration might also contribute to disorder in halloysite. Low rainfall or leaching promotes high solution-silica activity and facilitates halloysite formation, whereas high precipitation or leaching promotes low silica activity, favouring SRO material formation (Parfitt and Kimble 1989). Like precipitation, temperature also plays a role in the formation of SRO or crystalline minerals, with crystallisation promoted by higher temperatures (Talibudeen and Goulding 1983; Schwertmann 1985). SRO minerals are more persistent under a low soil temperature as crystallisation is hindered by a low input of thermal energy. Therefore, we hypothesised that thermal energy radiated by sulphide existing in the crater and the translocation process affected the transformation of the minerals in the crater. Climatic conditions and their effects on the degree of leaching and soil solution chemistry (toposequences) play an important role in volcanic material weathering pathways and secondary mineral neogenesis.

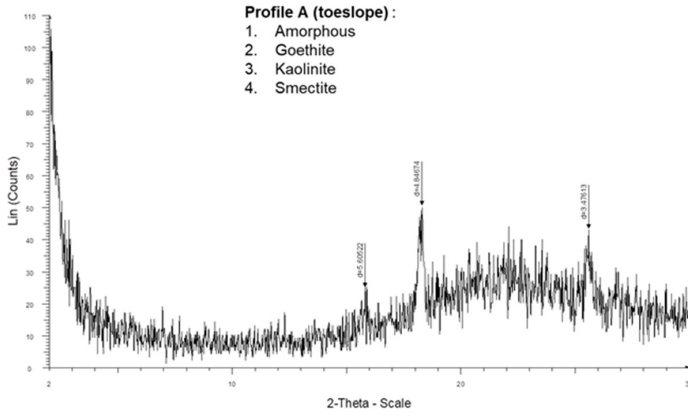

(a)

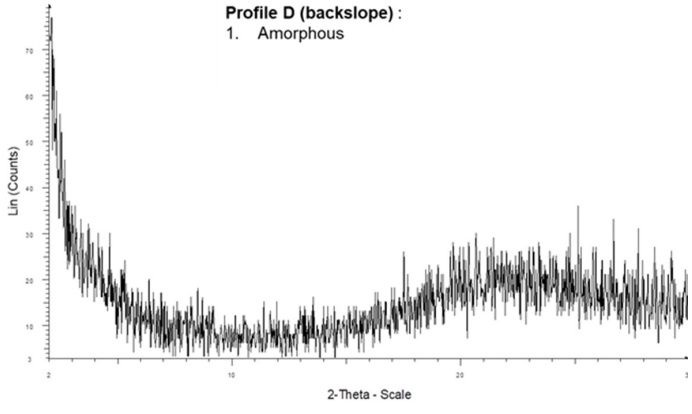

(b)

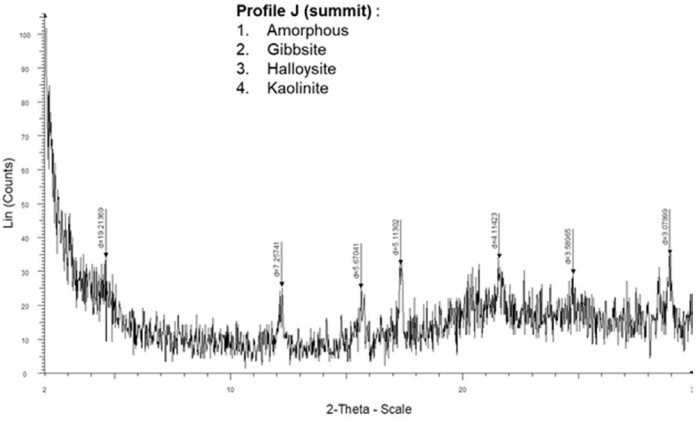

Figure 6. X-ray diffractograms for random powder mounts of Mg^{2+} saturation and glycerol solvation, clay fractions from surface horizons of each profile: (a) Profile A (toeslope), (b) Profile D (backslope), and (c) Profile J (summit)

Scanning Electron Microscope (SEM)

Further observations focused on three sample points on very fine sand fractions, i.e. A profile (toeslope) with 121x and 365x magnification in 20 µm size fractions, D profile (backslope) with 131x and 358x magnification in 20 µm size fractions, and J profile (summit) with 159x and 292x magnification in 30 µm size fraction, as shown in Figure 7.

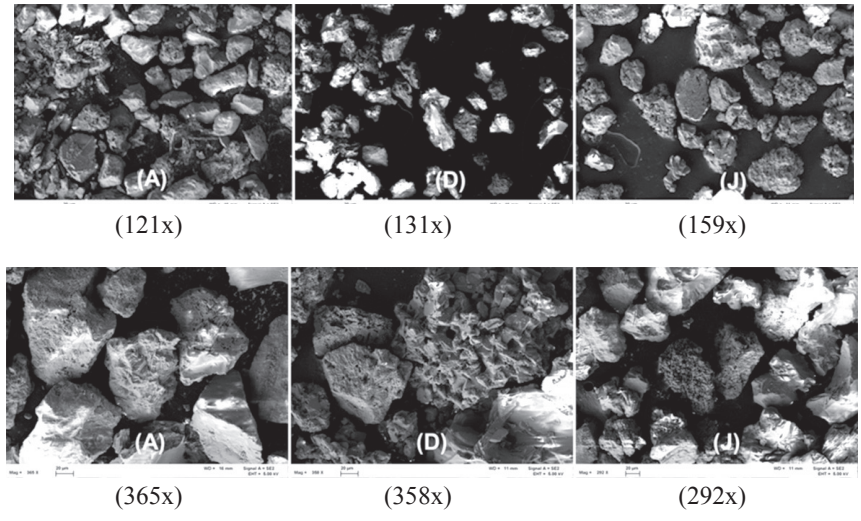

Figure 7. SEM images of sample profiles (A), (D), and (J) : A profile observed with 121x and 365 magnification, D profile observed with 131x and 368 magnification, and J profile observed with 159x and 292 magnification

The observation showed both fresh and weathered materials with Profile A being dominated by weathered materials due to deposit accumulation from the top sequence. Otherwise, the high temperature in the crater (as geothermal activity) also played an important role in the acceleration of materials weathering.

Visual Observations

Visual observations of surface rock along Ratu Crater toposequence are shown in Figure 8. The high temperature fluctuations due to geothermal activities swelled it vertically and horizontally, creating a crack and splitting the rock as shown in images A and B. Otherwise, the extreme temperature fluctuations split the top layer of the rock faster than the under layer, creating radial weathering shown in images C and D. Buol *et al.* (2011) stated that weathering is physical and chemical disintegration and decomposition of rocks, which occur due to the minerals not being in balance under conditions of extreme temperature, pressure, and humidity.

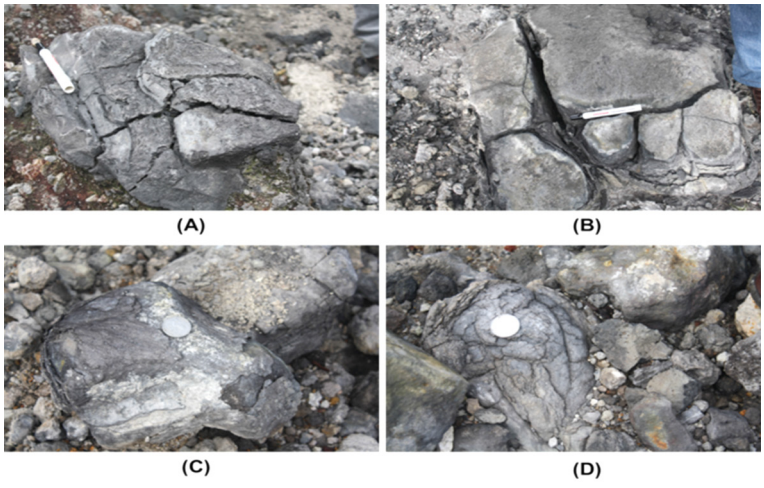

Figure 8. Rock weathering on Ratu Crater toposequences of Tangkuban Parahu volcano

CONCLUSION

Geothermal activities played a role primarily in creating specific conditions at the geothermal and surrounding location of the study, mainly at a very high ambient temperature and very acidic pH. Meanwhile, the topographic gradient (toposequence) played a role mainly in the process of mineral leaching. Geothermal activities and crater toposequence affected the composition of secondary minerals resulting in the toeslope profile being dominated by crystalline minerals (type 1: 1 and 2: 1). This was caused by high deposit accumulation from the leaching process, extremely fluctuating temperatures, very acidic pH and specific chemical content in the geothermal environment of the crater. The backslope was dominated by amorphous (non crystalline) minerals due to high intensity of leaching while the summit was dominated by amorphous and type 1: 1 minerals due to relatively lower temperatures that supported the formation of amorphous minerals. Mineralogical analysis showed that the sand fractions of heavy minerals (specific gravity > 2.87) were opaque, augite, and hipersten while the light minerals (specific gravity < 2.87) were volcanic glass, zeolite, andesin, labradorite, bytownite and rock fragments. Extraction with oxalate and pyrophosphate showed the highest mineral content of allophane (1.414 %), imogolite (0.391 %), and ferrihydrite (2,091 %) was in Profile D (backslope). The lowest content was found in Profile A (toeslope), which had a smaller content than Profile J (summit). XRD analysis results (no treatment) showed that all profiles A, B, D, G, J had almost the same reflection pattern consisting of calcite (3.03 Å), cristobalite (4.04 Å), feldspar (3.1-3.25 Å, gibbsite (4.85 Å), kaolinite (7.1 Å) and quartz (3.34, 4.27 Å). The mechanism and formation of secondary minerals in the Ratu Crater of TangkubanParahu volcano are summarised in Figure 10.

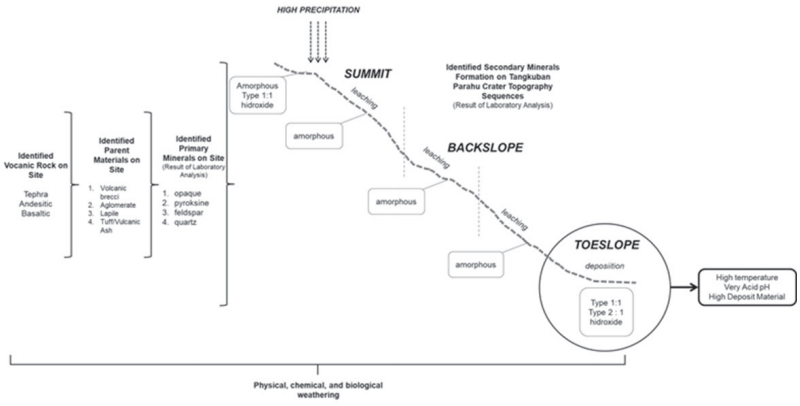

Figure 10. Mechanism and formation of secondary minerals on Ratu Crater toposequences of Tangkuban Parahu volcano

ACKNOWLEDGEMENT

We would like to thank soil laboratory staff of Idaho University, all supporting academic staff and the anonymous reviewers of this paper for their constructive comments and suggestions. This research was funded by Sandwich-Like Program from The Ministry of Higher Education and Technology, Indonesia.

REFERENCES

Buol, S. W., Southard, R. J., Graham, R. C., & McDaniel, P. A. (2011). *Soil Genesis and Classification: Sixth Edition.* Soil Genesis and Classification: Sixth Edition. Wiley-Blackwell. https://doi.org/10.1002/9780470960622

Churchman, G. J. (1990). Relevance of different intercalation tests for distinguishing halloysite from kaolinite in soils. *Clays & Clay Minerals.* 38(6), 591-599. Retrieved from www.clays.org/journal/archive/volume 38/38-6-591.pdf. https://doi.org/10.1346/CCMN.1990.0380604.

Dahlgren, R. A. (1994). Weathering, Soils & Paleosols. *Journal of Environmental Quality,* 23(2), 389–390. https:/ /doi.org /10.2134/jeq1994. 00472425002300020031x.

Dahlgren, R. A., Boettinger, J. L., Huntington, G. L., & Amundson, R. G. (1997). Soil development along an elevational transect in the western Sierra Nevada, California. *Geoderma,* 78(3–4), 207–236. https://doi.org/10.1016/S0016-7061(97)00034-7

McIntosh, P. D. (1979). Halloysite in a New Zealand tephra and paleosol less than 2500 years old. *New Zealand Journal of Science*, 22(1), 49–54.

Parfitt, R. L., & Childs, C. W. (1988). Estimation of forms of fe and al: A review, and analysis of contrasting soils by dissolution and moessbauer methods. *Australian Journal of Soil Research*, 26(1), 121–144. https://doi.org/10.1071/SR9880121

Parfitt, R. L., & Kimble, J. M. (1989). Conditions for Formation of Allophane in Soils. *Soil Science Society of America Journal*, 53(3), 971–977. https://doi.org/10.2136/sssaj1989.03615995005300030057x

Parfitt, R. L., Russell, M., & Orbell, G. E. (1983). Weathering sequence of soils from volcanic ash involving allophane and halloysite, New Zealand. *Geoderma,* 29(1), 41–57 https://doi.org/10.1016/0016-7061(83)90029-0

Rasmussen, C., Matsuyama, N., Dahlgren, R. A., Southard, R. J., & Brauer, N. (2007). Soil Genesis and Mineral Transformation Across an Environmental Gradient on Andesitic Lahar. *Soil Science Society of America Journal*, 71(1), 225–237. https://doi.org/10.2136/sssaj2006.0100

Schwertmann, U. (1985). Formation of Secondary Iron Oxides in Various Environments. In *The Chemistry of Weathering* (pp. 119–120). Springer Netherlands. https://doi.org/10.1007/978-94-009-5333-8_7

Shoji, S. (1985). Genesis and properties of non-allophanic andisols in Japan. *Applied Clay Science*, 1(1–2), 83–88. https://doi.org/10.1016/0169-1317(85)90564-2

Singleton, P. L., McLeod, M., & Percival, H. J. (1989). Allophane and halloysite content and soil solution silicon in soils fromrhyolitic volcanic material, new zealand. *Australian Journal of Soil Research,* 27(1), 67–77. https://doi.org/10.1071/SR9890067

Soil Survey Staff. (2014). *Kellogg Soil Survey Laboratory Methods Manual. Soil Survey Investigations Report No. 42, Version 5.0*. R. Burt and Soil Survey Staff (ed.). U.S. Department of Agriculture, Natural Resources Conservation Service.

Soma, M., Churchman, G. J., & Theng, B. K. G. (1992). X-ray photoelectron spectroscopic analysis of halloysites with different composition and particle morphology. *Clay Minerals*, 27(4), 413–421. https://doi.org/10.1180/claymin.1992.027.4.02

Talibudeen, O., & Goulding, K. W. T. (1983). Apparent charge heterogeneity in kaolins in relation to their 2:1 phyllosilicate content. *Clays & Clay Minerals,* 31(2), 137–142. https://doi.org/10.1346/CCMN.1983.0310208

Tan, K. H. (2010). P*rinciples of Soil Chemistry. Principles of Soil Chemistry*. CRC Press. https://doi.org/10.1201/9781439894606

Lal, R. (2017). Variable Charge Soils: Mineralogy and Chemistry. In *Encyclopedia of Soil Science, Third Edition.* (pp. 2432–2439). CRC Press. https://doi.org/10.1081/e-ess3-120053756

Van Zuidam, R. A. (1986). *Aerial photo-interpretation in terrain analysis and geomorphologic mapping.* Aerial Photo-Interpretation in Terrain Analysis and Geomorphologic Mapping. Smits Publishers, The Hague. https://doi.org/10.1016/0012-8252(88)90100-6

Weaver, R. M., Syers, J. K., & Jackson, M. L. (1968). Determination of Silica in Citrate-Bicarbonate-Dithionite Extracts of *Soils. Soil Science Society of America Journal*. 32(4), 497–501. https://doi.org/10.2136/sssaj1968.03615995003200040023x

Whittig, L. D., & Allardice, W. R. (2018). *X-Ray Diffraction Techniques* (pp. 331–362). https://doi.org/10.2136/sssabookser5.1.2ed.c12